Fitting Resolved Modes using GONG, MDI and HMI Observations.

S.G. Korzennik

Harvard-Smithsonian Center for Astrophysics, Cambridge, MA

Methodology

- Fit all available data since 1995, using my state of the art fitting methodology.
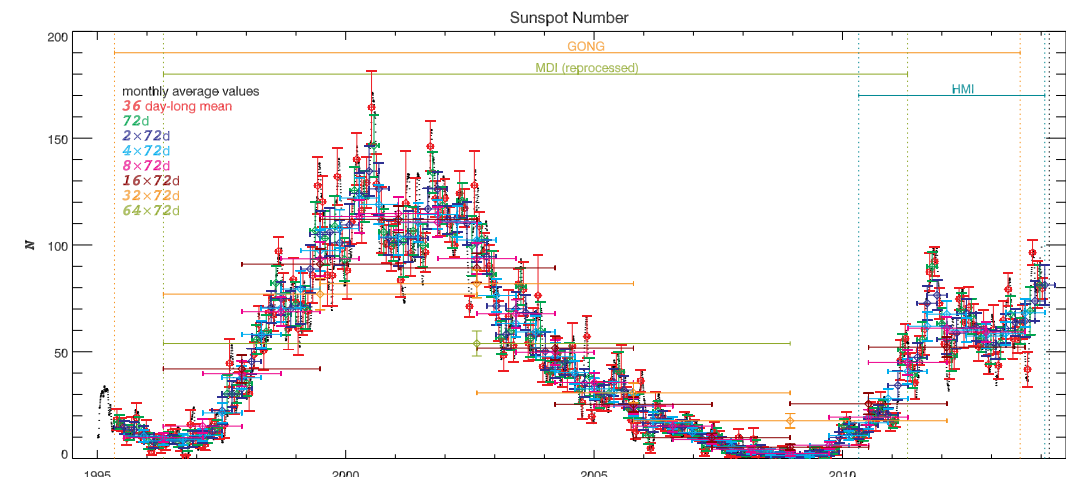

Fig. 1: Activity index, i.e., sunspot number, over the past 19 years and its mean value for the different fitted epochs.

▷ Simultaneous fitting of all m (individual peaks) that includes: asymmetric peak profile, complete leakage matrix, sanity rejection threshold, mode contamination

▷ Resolve modes for $0 \le \ell \le 300$, using time series of varying lengths, from 36-day long to 64×72-day long: 36, 72, 2×72, 4×72-day long, etc...
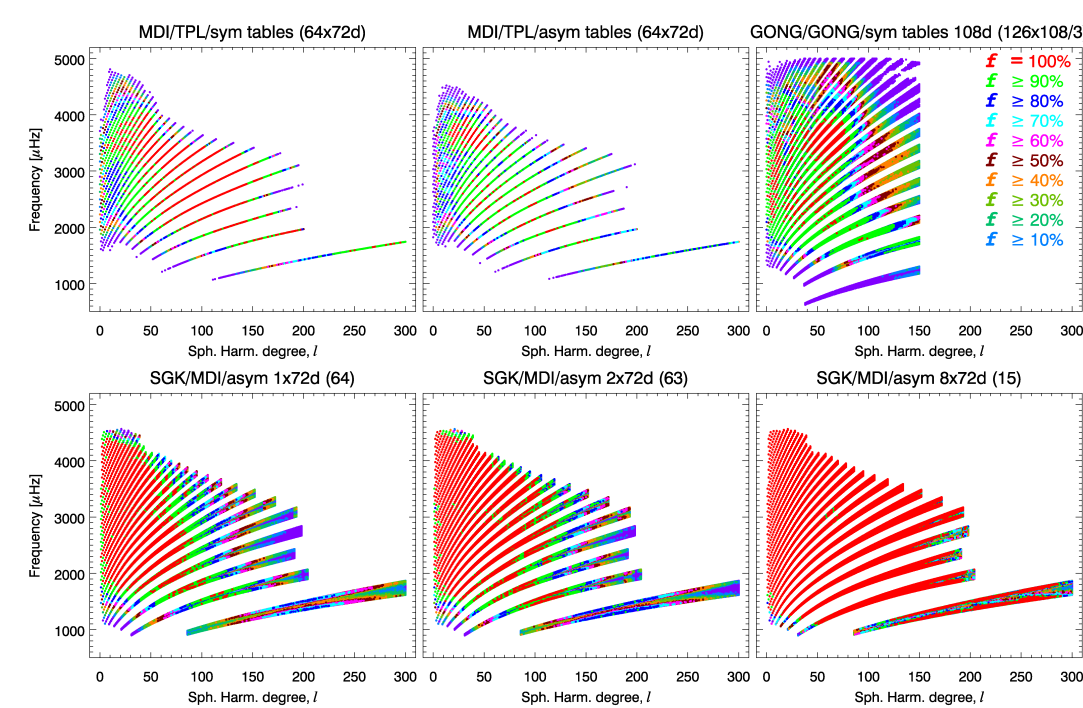
Attrition Rate

Fig. 2: Fitting attrition rate for different fitting methodologies.

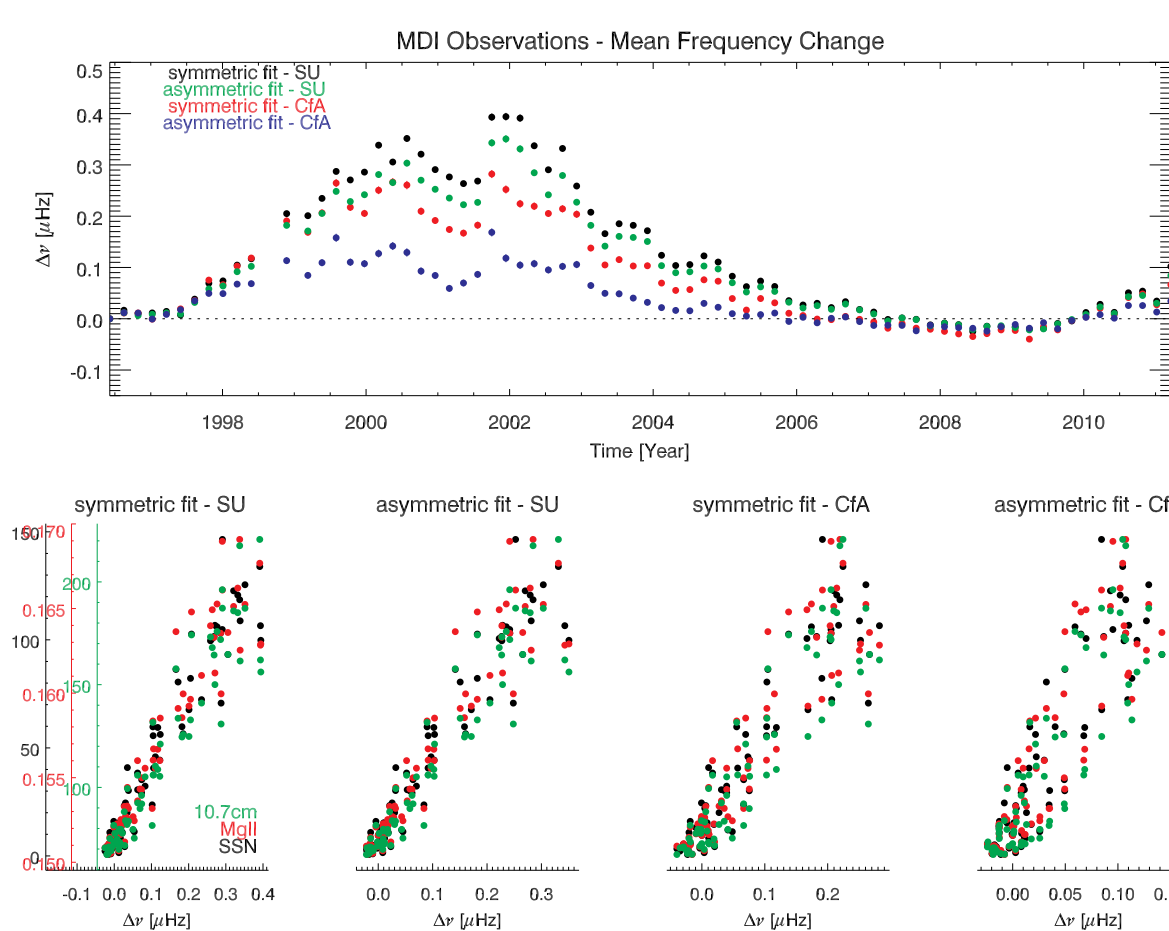## Changes in Mode Parameters

Frequency, $\delta\nu$

Fig. 3: Top panel: mean frequency change with respect to epoch, when fitting MDI observations using symmetric or asymmetric fits, produced by the MDI project (SU) or by my own independent fitting (CfA). Bottom panels: the mean changes compared to three solar activity indices.
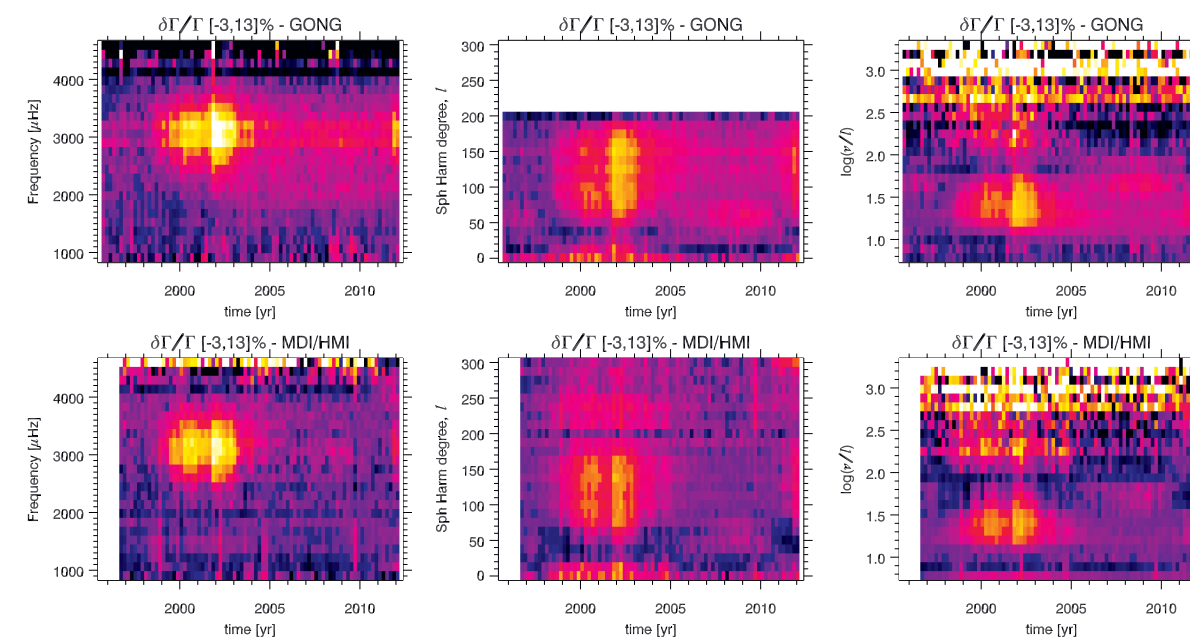
Changes in FWHM, $\delta\Gamma/\Gamma$

Fig. 4: Change in FWHM, $\delta\Gamma/\Gamma$ as a function of epoch –hence solar activity– and ν, ℓ, or $\log(\nu/L)$. The top row shows results from my fitting to GONG observations, the bottom row from my fitting to MDI & HMI observations.
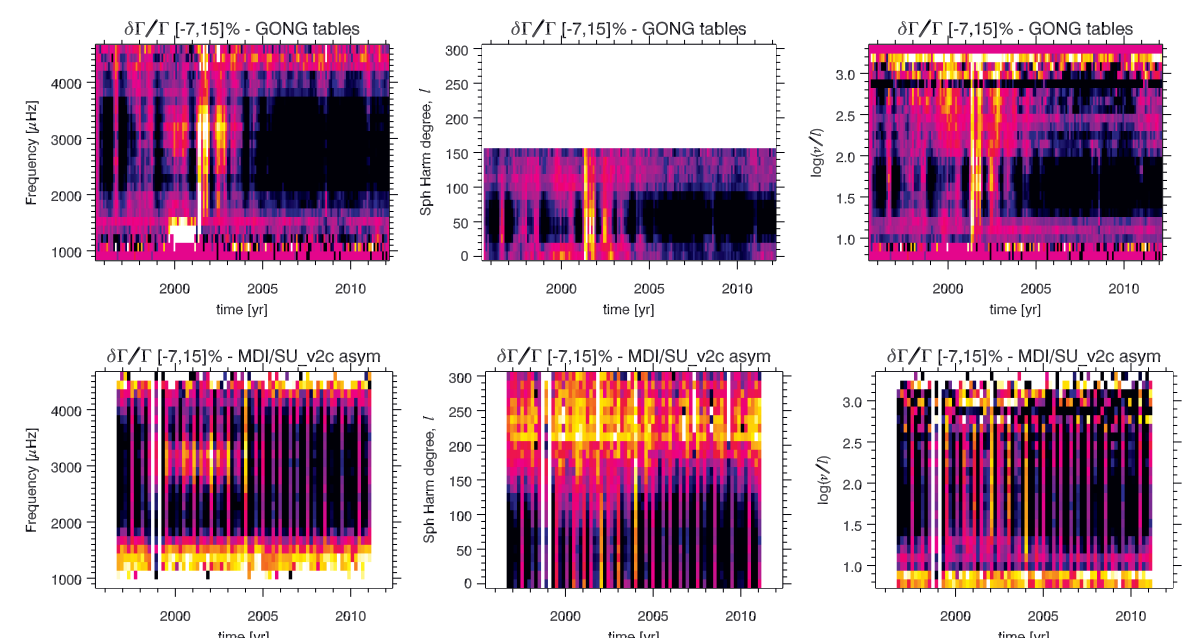

Fig. 5: Change in FWHM, $\delta\Gamma/\Gamma$, seen in the GONG project tables (top) and in the MDI project tables, (asymmetric fit, v2, bottom)
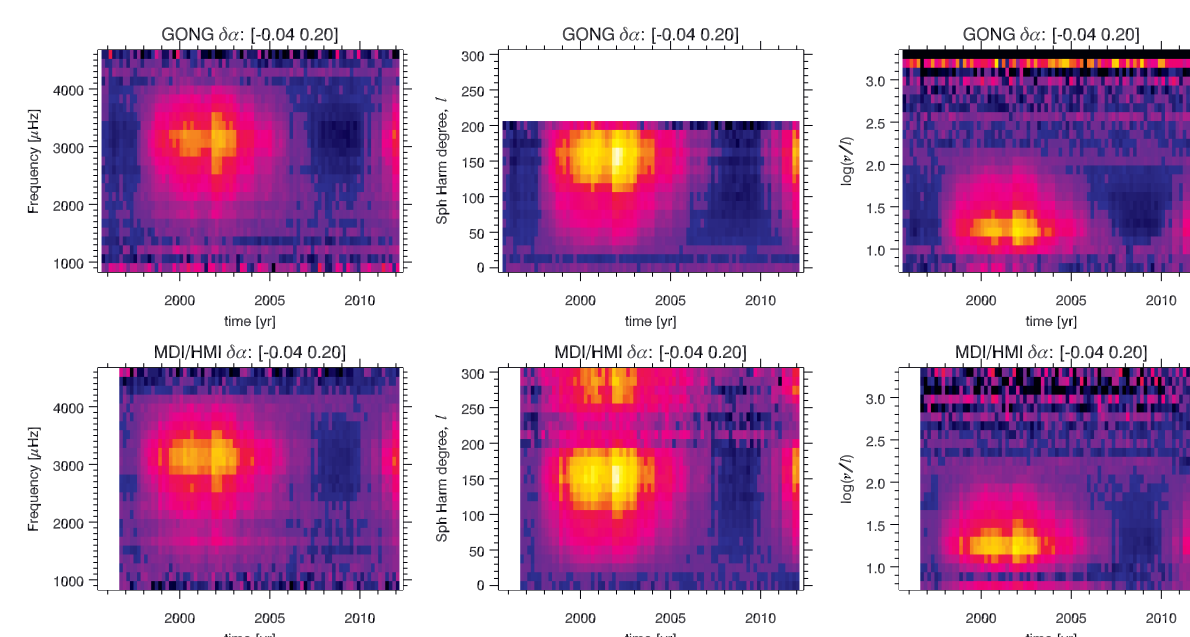
Asymmetry, $\delta\alpha$

Fig. 6: Change in asymmetry, $\delta\alpha$, as a function of epoch –hence solar activity– and ν, ℓ, or $\log(\nu/L)$. The top row shows results from my fitting to GONG observations, the bottom row from my fitting to MDI & HMI observations.
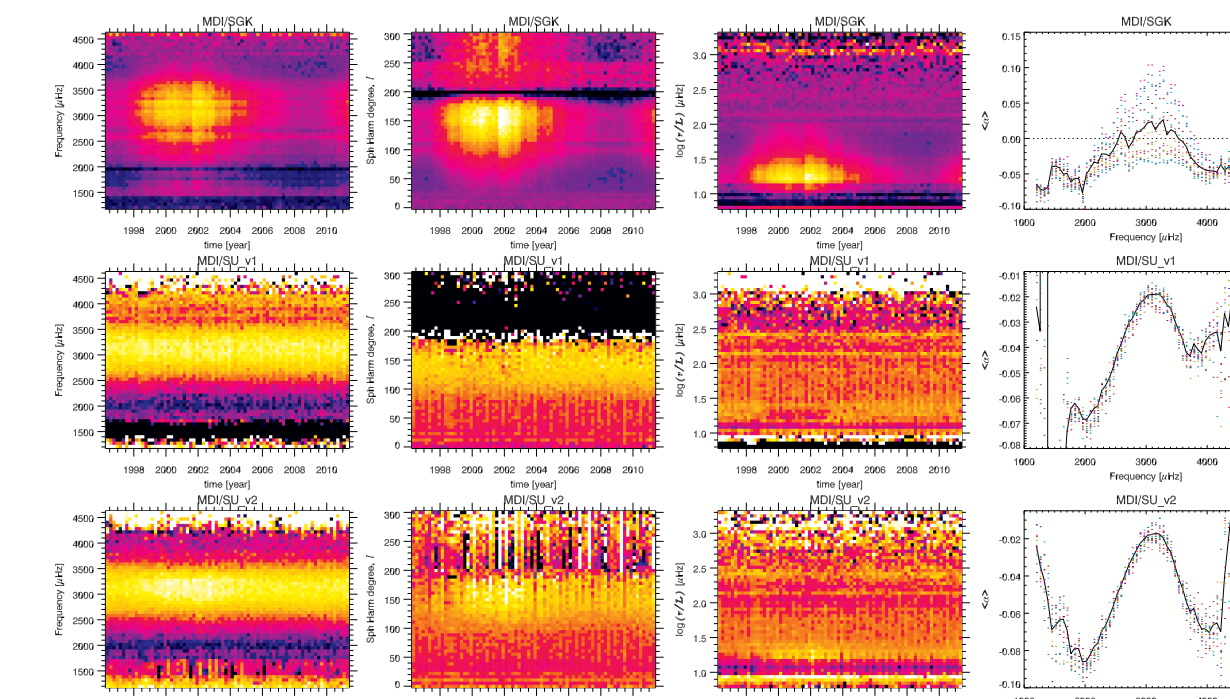

Fig. 7: Change in asymmetry, $\delta\alpha$, seen in MDI project tables, once converted to my convention, compared to results of my fitting (top row). Middle row is MDI project tables v1 (obsolete, b/c of a bug), bottom row is for new release, aka v2

Changes in Solar Rotation with Activity
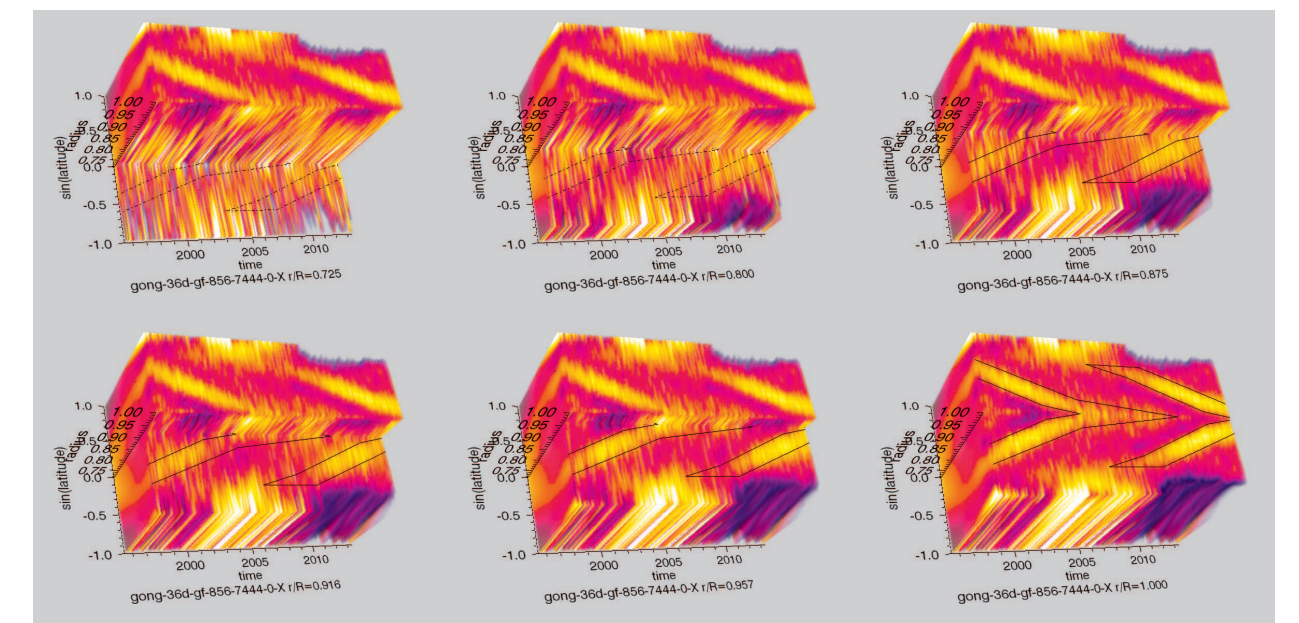
Residual Rotation

Fig. 8: Rotation rate in the top 28.7% of the solar interior, as a function of time, latitude and depth, after subtracting the mean rotation profile for Cycle 23. Each panel shows a cut at a given depth, and the outline of the surface torsional oscillation (faster than the mean).
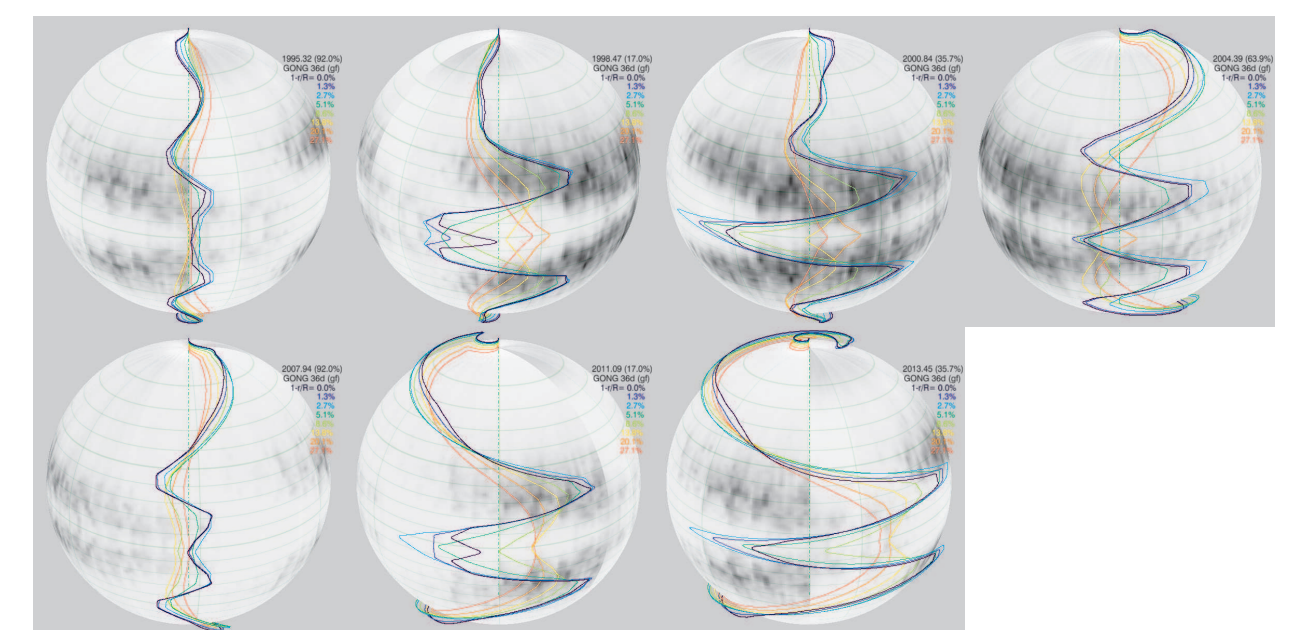
Comparison of Cycle 23 to Cycle 24

Fig. 9: Propagation diagrams at 7 epochs. The colored lines show the torsional displacement with respect to the mean rotation profile at 8 depths throughout the convection zone. A rotating butterfly diagram is wrapped onto the sphere. The top row shows the end of Cycle 22 and Cycle 23, the bottom row shows teh same epochs as the top row except for the end of Cycle 23 and for Cycle 24. The propagation diagrams in the bottom row clearly show that the signature of the torsional oscillations is stronger during Cycle 24 than Cycle 23 (robust) and that the rotation rate in the lower part of the convection zone during Cycle 24 has a different equatorial component than during Cycle 23 (weaker result).

Acknowledgments